Excited State Dynamics in Recombinant Water-Soluble Chlorophyll Proteins (WSCP) from Cauliflower Investigated by Transient Fluorescence Spectroscopy

ARTICLE *in* THE JOURNAL OF PHYSICAL CHEMISTRY B · NOVEMBER 2008

Impact Factor: 3.3 · DOI: 10.1021/jp8024057 · Source: PubMed

10 AUTHORS, INCLUDING:

Franz-Josef Schmitt
Technische Universität Berlin
55 PUBLICATIONS **439** CITATIONS
SEE PROFILE

Christoph Theiss
Technische Universität Berlin
33 PUBLICATIONS **322** CITATIONS
SEE PROFILE

Thomas Renger
Johannes Kepler University Linz
95 PUBLICATIONS **3,197** CITATIONS
SEE PROFILE

Harald Paulsen
Johannes Gutenberg-Universität Mainz
120 PUBLICATIONS **3,488** CITATIONS
SEE PROFILE

Excited State Dynamics in Recombinant Water-Soluble Chlorophyll Proteins (WSCP) from Cauliflower Investigated by Transient Fluorescence Spectroscopy

F.-J. Schmitt,[†] I. Trostmann,[§] C. Theiss,[†] J. Pieper,[‡] T. Renger,[||] J. Fuesers,[†] E. H. Hubrich,[†] H. Paulsen,[§] H. J. Eichler,[†] and G. Renger*[,‡]

Institute of Optics and Atomic Physics, Berlin Institute of Technology, Berlin, Germany, Max Volmer Laboratory for Biophysical Chemistry, Berlin Institute of Technology, Berlin, Germany, Institute of General Botany, Johannes Gutenberg University Mainz, Mainz, Germany, Institute for Chemistry and Biochemistry, Free University Berlin, Berlin, Germany

Received: March 19, 2008; Revised Manuscript Received: July 2, 2008

The present study describes the fluorescence emission properties of recombinant water-soluble chlorophyll (Chl) protein (WSCP) complexes reconstituted with either Chl *a* or Chl *b* alone (Chl *a* only or Chl *b* only WSCP, respectively) or mixtures of both pigments at different stoichiometrical ratios. Detailed investigations were performed with time and space correlated ps fluorescence spectroscopy within the temperature range from 10 to 295 K. The following points were found: (a) The emission spectra at room temperature (295 K) are well characterized by bands with a dominating Lorentzian profile broadened due to phonon scattering and peak positions located at 677, 684 and 693 nm in the case of Chl *a* only WSCP and at 665, 675 and 689 nm for Chl *b* only WSCP. In addition, all spectra contain minor bands in the longer wavelength region. (b) The emission spectra at 10 K of samples suspended in buffer containing 50% glycerol are dominated by bands peaking at 668 nm for Chl *b* only WSCP and at 685 nm for Chl *a* only WSCP and samples reconstituted with mixtures of Chl *a* and Chl *b*. (c) At 10 K and in buffer with 50% glycerol the decay kinetics of WSCP samples with Chl *a* only are dominated by a component with a time constant of 6.2 (± 0.2) ns at 685 nm while those of WSCP containing mixtures of Chl *a* and Chl *b* are characterized by a slightly shorter value of 6.0 (± 0.2) ns. WSCP containing Chl *b* only exhibits a distinctly longer value of 7.0 (± 0.3) ns at an emission wavelength of 668 nm. (d) The decay associated emission spectra at 10 K of all samples exhibit at least 3 decay components with time constants of 80−120 ps, 2−4 ns and 6−7 ns in 50% glycerol. These results are consistently described within the framework of our previously presented model (*J. Phys. Chem. B* **2007**, *111*, No. 46, 13325; *J. Phys. Chem. B* **2007**, *111*, No. 35, 10487)[1,2] for the structural motifs of chlorophyll binding to the tetrameric protein matrix of WSCP. It is shown that formation of strongly coupled open sandwich dimers does not lead to quenching of ^{1}Chl *a** or ^{1}Chl *b**.

Introduction

Pigment−protein complexes are the essential constituents of all biological organisms that are able to transform solar radiation into free (Gibbs) energy as the driving force for living processes. Photosynthesis appears to be the most important process in solar energy exploitation of the biosphere.[3] All photosynthetic organisms contain bacteriochlorophyll (BChl) (anoxygenic bacteria) or chlorophyll (Chl) (all oxygen evolving species) molecules as the essential pigments of the apparatus. The pigments are bound to protein matrices in a well-defined manner in order to functionalize them as cofactors for different physiological demands. This goal is achieved by establishing pigment arrangements at suitable mutual orientations and distances and tuning of the optical properties by the protein environment. Basically two different types of pigment- protein complexes are essential constituents of the photosynthetic apparatus: (i) antenna complexes and (ii) reaction centers (RCs) either in anoxygenic bacteria or in photosystem I (PS I) and photosystem II (PS II) of oxygen evolving cyanobacteria and plants (for a review, see ref 4 and references therein).

The antenna complexes permit a most efficient adaptation of anoxygenic photosynthetic bacteria,[5] cyanobacteria[6] and plants[7] to different and widely varying illumination conditions. At low light intensities the few electronically excited singlet states are funnelled with high efficiency to the photochemically active pigment of the RCs/PSs where the photochemical charge separation takes place.[8−10] An opposite effect is induced under strong illumination; i.e., the radiationless decay of the superfluous excited singlet states is stimulated by opening dissipative channels, and in addition, (bacterio)chlorophyll triplets formed via intersystem crossing are effectively quenched by carotenoids (Cars).[11]

In contrast to the reactions in the antenna, the excited states in RCs, PS I and PS II are transformed into electrochemical Gibbs energy via electron transfer thus giving rise to formation of the primary cation−anion radical pairs followed by stabilization steps under the participation of secondary acceptor components (for reviews, see refs 8−10 and references therein).

In plants both of these types of pigment−protein complexes (antennae and photosystems) are highly hydrophobic and incorporated into the thylakoid membrane as integral proteins.

In addition to these operational units of the photosynthetic apparatus, many plants (Brassicaceae, Polygonaceae, Chenopo-

* Author for correspondence.
[†] Institute of Optics and Atomic Physics, Berlin Institute of Technology.
[§] Institute of General Botany, Johannes Gutenberg University Mainz.
[‡] Max Volmer Laboratory for Biophysical Chemistry, Berlin Institute of Technology.
[||] Institute for Chemistry and Biochemistry, Free University Berlin.

10.1021/jp8024057 CCC: $40.75
Published on Web 10/10/2008

diaceae, and Amaranthaceae) contain another type of chlorophyll-binding proteins that are characterized by entirely different properties. First of all, these complexes are water-soluble and not bound to thylakoids. Therefore, these highly hydrophilic chlorophyll proteins are denoted water-soluble chlorophyll proteins (WSCPs). Second, the WSCPs bind no more than one chlorophyll molecule per polypeptide subunit and none of them was found to contain Cars.[12]

The WSCP family can be classified into complexes that are prone to photoconversion upon illumination, giving rise to a red shift of the absorption spectrum (Class I), and those remaining spectrally invariant (Class II) (for a review, see ref 13). Upon pigment binding the WSCPs oligomerize with tetramers being the dominating aggregation form.[12,14]

The functional role of the WSCPs is not yet clarified. Based on their specific properties it is highly unlikely that WSCPs are involved in the primary processes of photosynthesis. One striking feature is the marked stimulation of WSCP expression upon different types of stress like drought,[15] salinity,[16] and heat[17] or leaf detachment.[18] This finding points to a protective role against degradative processes of the photosynthetic apparatus. When taking into account the high affinity for chlorophyll binding[12,13] it appears attractive to speculate on a regulatory role in controlling pigment synthesis or decay pathway(s), thus avoiding or diminishing deleterious photodynamic effects.

The idea of a function in the metabolic pathway of chlorophyll formation[12,19] assumes that WSCP can bind Chl precursor(s) while the hypothesis on a role in the catabolic degradation pathway assumes that WSCP traps chlorophyll during senescence of leaves and transports the pigments to the inner envelope membrane of chloroplasts where the enzyme chlorophyllase initiates the degradation process.[20,21] A support of the former proposal might be the finding that a WSCP homologue from barley (*Hordeum vulgare*) which is able to bind chlorophyllide accumulates in chloroplasts after exposure of etiolated seedlings to light;[19] however, this notion has not been confirmed so far.

Regardless of the detailed function of WSCP, it seems clear that the mode of chlorophyll binding to the protein matrix is an essential parameter for the type of function. Until recently, the arrangement of the Chls in WSCPs was an open question. Detailed spectroscopic studies and theoretical analyses led to the conclusion that recombinant cauliflower WSCP reconstituted with different chlorophylls (Chl *a*, Chl *b*, Chl *d*) binds the pigments in form of an excitonically strongly coupled dimer with an "open sandwich" geometry.[1,2,22] Our model calculations resulted in an open sandwich configuration with a tilt angle of about 30° for Chl *a* homodimers, Chl *b* homodimers and Chl *a*/Chl *b* heterodimers in WSCP.[2] This model also consistently describes the fast excited-state dynamics of Chl *a*/Chl *b* heterodimers on the fs and ps time scale.[1] It was very exciting to see that the first published X-ray diffraction crystal structure of a Class II WSCP at 2.0 Å resolution[23] shows Chl binding in the predicted open sandwich geometry with a tilt angle of 27°. The possible functional role of this geometry is not yet clarified. In this respect it is interesting to note that the excitonic coupling of a chlorophyll dimer in this array gives rise to an oscillator strength that is significantly higher for the upper than the lower exciton band.[1,2,22] This phenomenon is just the opposite of the excitonically coupled "special pair" P in bacterial RCs and similar arrays of P700 in PS I and P680 in PS II where the lower exciton band carries most of the oscillator strength. These special pairs are tailored as cofactors for the process of primary charge separation.[8−10] Strongly coupled dimers with similar structure also occur in antennae, e.g., LH1 and LH2.[5]

Although WSCPs lack carotenoids (Cars), the chlorophylls (Chls) bound to this protein exhibit a surprisingly high stability against photobleaching compared with that of pigment solutions.[12] The formation of a Chl dimer[24] or the interaction with the protein matrix[25] could lead to a strong quenching of ^{1}Chl* states which would explain the photostability because the triplet states population ^{3}Chl is drastically diminished.

The lifetime of ^{1}Chl *a** was found to be about 200 ps in solubilized cytochrome b_6/f, which contains a single Chl *a* molecule of unknown function,[26,27] as compared to about 4.5 ns of Chl solutions and trimeric LHC II complexes.[28] This quenching of ^{1}Chl* in Cytb_6/f is ascribed to interaction of the pigment with aromatic amino acid residues.[27] The striking phenomenon of drastically shortened lifetimes of ^{1}Chl* in a natural Chl-binding protein is an attractive feature and suggests considering the existence of an analogous phenomenon in WSCP because structural data reveal the presence of aromatic amino acid residues close to the Chl binding sites.[23]

In order to check for these possibilities, the excited-state dynamics were analyzed in recombinant WSCP from cauliflower that is reconstituted either with Chl *a* or Chl *b* only or with Chl *a*:Chl *b* mixtures. This sample material containing two chlorophyll molecules per protein tetramer was shown to be suitable for biophysical studies.[1,2] The present analyses were performed by using time-resolved fluorescence spectroscopy covering a wide temperature range.

The results obtained reveal that (i) the spectral properties and excited singlet state dynamics can be consistently described within the framework of our model of a protein tetramer binding excitonically coupled Chl dimers which was presented in refs 1 and 2, (ii) the open sandwich dimers in WSCP do not act as quenchers of ^{1}Chl* compared with Chl in solution or detergent micelles,[28] and (iii) the fluorescence dynamics of WSCP exhibits at least three decay components at 10 K and is strongly temperature-dependent.

Materials and Methods

Sample Material. ***Protein.*** Recombinant WSCP from cauliflower (*Brassica oleracea* var. botrytis) with an N-terminal hexahistidyl (His) tag was expressed as previously described.[12] Following induction of WSCP expression with IPTG, the growth temperature was reduced to 28 °C and protein expression was continued under these conditions overnight. After cell lysis and centrifugation, the supernatant containing soluble WSCP was stored in aliquots at −20 °C to be used for sample preparation.

Pigment. Total pigment extract was obtained from pea plants as previously described.[29] Purified Chl *a* and *b* were prepared as described in Hobe et al.[30] Aliquots of pigments were dried and stored at −20 °C in inert (nitrogen) atmosphere.

Reconstitution of Chl-WSCP. Reconstitution and purification of soluble WSCP was performed simultaneously by binding the protein to a Chelating Sepharose™ Fast Flow (Amersham Biosciences) column charged with Ni^{2+} ions and equilibrated with 50 mM Na-phosphate pH 7.8. The sample was filtered before loading on the column at 2 mg WSCP per ml of column material. After removal of contaminating bacterial proteins by washing with 10 column volumes of 50 mM Na-phosphate pH 7.8 and following equilibration of the column with 5 column volumes of 50 mM Na-phosphate pH 7.8/12.5% sucrose/1% octyl-β-D-glucopyranosid (NaP-OG-buffer), the protein was incubated with a 5-fold molar excess of Chl (either Chl *a* or Chl *b* or total pigment extract) presolubilized in 100% ethanol at 10 mg/ml and then diluted 20-fold with NaP-OG-buffer. The pigment solution was thoroughly dispersed with the column material and then incubated for 1−2 h

at room temperature under protection from light. Unbound Chl was removed by a thorough wash with 30 column volumes of the same buffer. After detergent removal by washing with 10 column volumes of 50 mM Na-phosphate pH 7.8, the purified and reconstituted pigmented protein was eluted from the Ni^{2+}-column with 20 mM Na-phosphate pH 7.8/300 mM imidazole/2 mM β-mercaptoethanol and subsequently concentrated in Centricon devices (30 kDa MW cutoff, Millipore), so that the sample had an OD at 673 nm of at least 1 at a path length of 2 mm. For fluorescence measurements the samples were diluted with elution buffer (room temperature measurements) or elution buffer and 50% glycerol (low temperature measurements) until a final concentration of 5 μM Chl was reached. Determination of the pigment to protein ratio was performed as described in Renger et al.[2] It should be noted that the Chl *a*:Chl *b* ratios mentioned in this study refer to the WSCP-bound pigments. These ratios were obtained during the respective reconstitutions and were dependent on the solubility of the chlorophylls in the pigment solution. The Chl *a*:Chl *b* ratio in the WSCP-complexes was determined by HPLC-analysis of the pigments, which were extracted with 2-butanol after destabilization of the complexes by adding 1% SDS (w/v), as described in ref 12 with some modifications described in ref 2.

Measurements. ***Time- and Wavelength-Resolved Fluorescence.*** The measurements were performed with the double correlated single photon counting fluorometer system that is described in detail in ref 31. This equipment permits simultaneous fluorescence monitoring in the time and wavelength domain.

In all measurements performed in this study a high signal-to-noise *S*/*N* ratio $\sim \sqrt{S} > 100$ was achieved for up to 30 wavelength sections with each of 5−10 nm spectral width, where *S* is proportional to the number of counts. Measurements at low temperatures were performed with a variable-temperature cryostat (10−300 K, CTI-Cryogenics 8001/8300). The wavelength resolution is achieved by a delay-line detector (Europhoton GmbH, Berlin). The total time-spread of the delay-line anode is 5.7 ns. A personal computer system via appropriate evaluation electronics (analog-to-digital-converters, constant fraction discriminators, multichannel analyzers, for details see also ref 32) transfers the signals of the two time-to-amplitude converters (one connected with the delay-line for the wavelength information and one connected to the microchannel-plate PMT for the time information) into a 2-dimensional matrix of 256 channels for the wavelength domain and 1024 channels for the time domain. Then 5−10 wavelength channels are binned in order to achieve *S*/*N* ratios of >100. The instrumental response function (IRF) was measured by detecting the attenuated excitation light scattered from a water-filled cuvette as used for measuring the sample fluorescence. The IRF of the system was found to have a full width at half-maximum (fwhm) of 100 ps.

A picosecond diode laser module was used for excitation at 632 nm (fwhm 60 ps; repetition frequency, 20 MHz; Becker & Hickl GmbH, Berlin, BHL-600). Fluorescence was detected at a right angle to the excitation beam. The scattered excitation light was suppressed by inserting a long-pass emission filter between the cuvette and the detector (640ALP, Omega Inc.). Excitation pulses in the spectral blue range at 430 and 460 nm were generated by a Ti:Sa-Oszillator (Tsunami, Spectra Physics) tunable between 720 and 980 nm and afterward frequency doubled in a thin BBO crystal to obtain ultrashort excitation pulses in the blue spectral range. Using a pulse picker system (Spectra Physics mod. 3980) the repetition rate of 82 MHz was reduced to 4 MHz.

Data Analysis. The fluorescence decay was analyzed by fitting of a multiexponential model employing the Levenberg−Marquardt algorithm for the minimization of the reduced χ^2 after deconvolution of the IRF:

$$F(t,\lambda) = \sum_{j=1}^{n} a_j(\lambda) e^{-t/\tau_j} \quad (1)$$

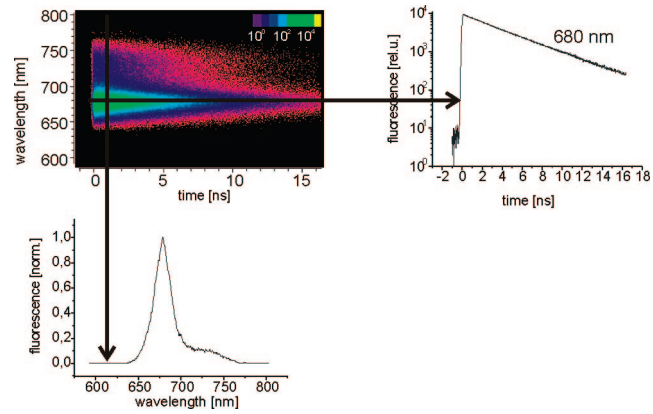

Figure 1. Color intensity plot (CIP) of a fluorescence measurement at 298 K on WSCP solution containing WSCP with a Chl *a*:Chl *b* ratio of 4.2:1 after excitation at 632 nm (for details, see text).

Results

Figure 1 shows a color intensity plot (CIP) of a typical fluorescence measurement performed at room temperature under 632 nm excitation (upper panel, left side). The CIP contains the time- and wavelength-resolved fluorescence emission data and provides information on (i) steady state fluorescence spectra and (ii) lifetimes and dynamics of different emitter states.

A vertical plot at a constant time *t* results in the time-resolved emission spectrum $F(t)$ (bottom panel) while a horizontal intersection gives the fluorescence decay at a constant emission wavelength λ (upper panel, right side). The spectral resolution of this spectrometer system is limited to about 2 nm due to the distance of the delay-line meanders.[32]

Fluorescence Spectra at Room Temperature and at 10 K. Figure 2 shows the normalized fluorescence spectra integrated over the time domain, i.e., the integral $\int_0^\infty F(\lambda,t)\,dt$ as a function of wavelength, of Chl *a* only WSCP (top panel) and Chl *b* only WSCP (bottom panel), respectively, measured at room temperature under excitation with 632 nm pulses.

In both cases (Chl *a* only and Chl *b* only WSCP) broad spectra are obtained that can be deconvoluted into three main bands of Lorentzian shape with maxima at 677, 684 and 693 nm in the case of Chl *a* only WSCP and at 665, 675 and 689 nm for Chl *b* only WSCP. In addition, minor bands are obtained in the long wavelength region that probably originate from the 0−1 vibrational transitions in the Q_y emission spectrum of the chlorophylls. The use of Lorentzian lineshapes appears to be justified by the fact that electron−phonon coupling leads to a symmetric, non-Gaussian tailing of the absorption and corresponding fluorescence bands of pigments embedded into amorphous protein matrices with thermal occupation of vibrational energy levels at elevated temperatures. Because of the generally broad distribution of protein phonon modes with a width of, e.g., $\sim$105 cm^{-1} in the case of LHCII[33] we assume that electron−phonon coupling is a main broadening mechanism at 293 K. In addition, a significant lifetime broadening of the optical bands can be expected at room temperature, which also leads to Lorentzian bands.[2]

The normalized time-integrated emission spectra of Chl *a* only and Chl *b* only WSCP presented in Figure 2 were obtained under

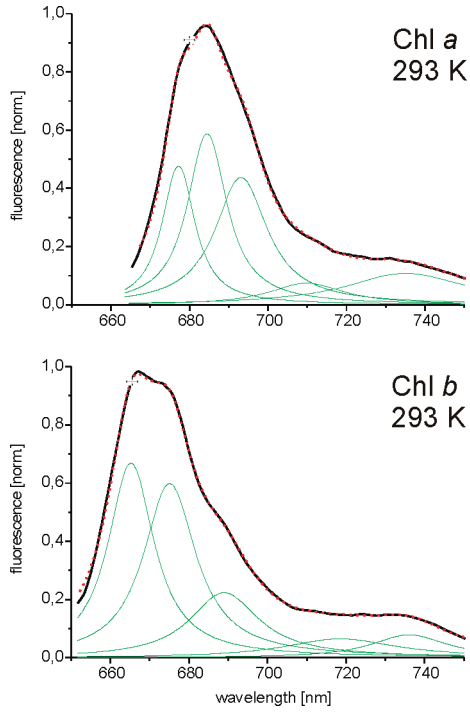

Figure 2. Normalized spectra of the integrated fluorescence $F(\lambda) = \int_0^\infty F(\lambda,t)\,dt$ of WSCP containing Chl *a* only (top panel) or Chl *b* only (bottom panel) at room temperature (black full-lined curve). Deconvolution into Lorentzians (thin-lined curves) was performed in frequency domain and the curves were rescaled to the wavelength region (the sum of all subbands is represented by the dotted curve). The crosses positioned near the emission maxima indicate the standard deviation of the wavelength positions of the integrated fluorescence spectrum.

excitation with 632 nm pulses. The shape should be independent of the excitation wavelength, since the equilibration of excited-state populations is much faster than the decay due to intersystem crossing, internal conversion and fluorescence.

However, an analogous feature is not necessarily expected for WSCP samples that are reconstituted with mixtures of Chl *a* and Chl *b* because in that case the sample ensemble contains homodimers (Chl *a* only and Chl *b* only) and Chl *a*/Chl *b* heterodimers. Therefore, measurements were performed on WSCP containing Chl *a*:Chl *b* at a ratio of 4.2:1 where the sample is preferentially excited in the Soret band of either Chl *a* (430 nm) or Chl *b* (460 nm). The results obtained are shown in Figure 3 and compared with the spectra taken from Figure 2 for Chl *a* only (dot-dashed curve) or Chl *b* only (dashed curve) WSCP.

Inspection of this data reveals that the emission in the region of Chl *b* (650 − 670 nm) is more pronounced under 460 nm illumination (full-lined curve) while less fluorescence is emitted in this region when the samples are excited at 430 nm (dotted curve). These features qualitatively reflect the existence of both Chl *a*/Chl *a* homo- and Chl *a*/Chl *b* heterodimers together with minor fractions of Chl *b*/Chl *b* homodimers within the overall assembly of WSCP complexes. At 430 nm the Chl *a*/Chl *a* homodimers and Chl *a*/Chl *b* heterodimers and at 460 nm the Chl *b*/Chl *b* homodimers and Chl *a*/Chl *b* heterodimers are preferentially excited. As the thermal equilibration between the two exciton states is faster than 1 ps in the strongly coupled and still faster than 8 ps in the weakly coupled heterodimers (see ref 1), the spectral shape of the heterodimer emission is expected to depend only slightly on the excitation wavelength. Therefore, a higher relative extent of emission emerges in the "red edge" (Chl *a*/Chl *b* heterodimers, Chl *a*/Chl *a* homodimers)

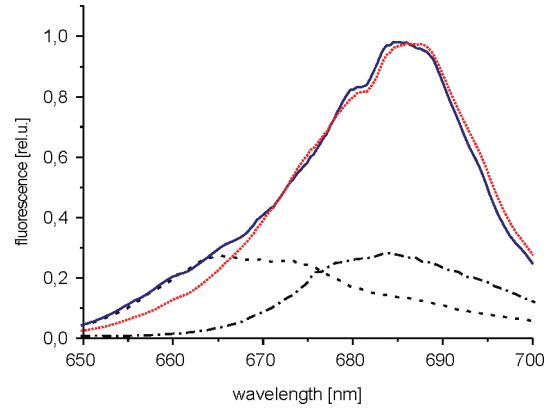

Figure 3. Normalized spectra of the integrated fluorescence $F(\lambda)$ at room temperature of WSCP containing Chl *a* and Chl *b* at a ratio of 4.2:1; excitation wavelength: 430 nm (dotted curve) and 460 nm (full-lined curve). The experimental spectra of Chl *a* only (dot-dashed curve) or Chl *b* only (dashed curve) of Figure 2 are depicted for comparison.

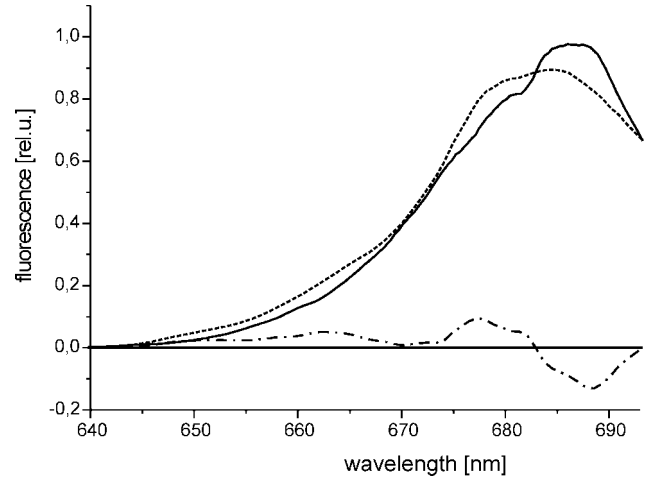

Figure 4. Normalized integral fluorescence spectrum of WSCP containing Chl *a* and Chl *b* at a ratio of 4.2:1 (full-lined curve), measured at room temperature, and the calculated sum of the corresponding spectra of WSCP containing Chl *b* only and Chl *a* only taken from Figure 3 and weighted with a ratio of 1:4.2 (dashed curve). Excitation wavelength: 632 nm. The dot-dashed curve is the difference between the dashed curve and the full-lined curve (see text for details).

under excitation at 430 nm and in the "Chl *b* region" (Chl *a*/Chl *b* heterodimers, Chl *b*/Chl *b* homodimers) under excitation at 460 nm. In order to illustrate the existence of mixtures of Chl *a*/Chl *a* and Chl *b*/Chl *b* homodimers and Chl *a*/Chl *b* heterodimers in the WSCP samples reconstituted with mixtures of Chl *a* and Chl *b*, the calculated sum of the emission spectra of Chl *a* only WSCP and Chl *b* only WSCP at relative contributions of 4.2:1 is compared with the experimental spectrum of the mixed WSCP sample with a 4.2:1 stoichiometry of Chl *a* and Chl *b*.

The results shown in Figure 4 reveal that marked differences exist between the normalized experimental spectrum $\int_0^\infty F(\lambda,t)\,dt$ (full-lined curve) and that calculated from the sum of the spectra taken from Figure 2 for WSCP containing Chl *b* only and Chl *a* only (dashed curve). The difference between both curves is illustrated by the dot-dashed curve.

Differences are seen in the region of both Chl *b* (665 nm) and Chl *a* (677 nm, 685 nm) emission. WSCP with a Chl *a*:Chl *b* ratio of 4.2:1 shows less intense fluorescence at 665 and 677 nm but more intense fluorescence at 685 nm than the weighted

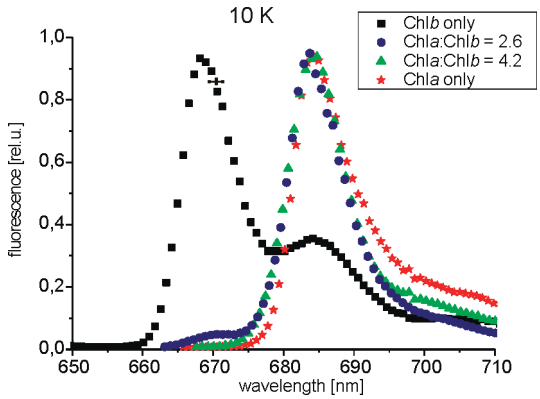

Figure 5. Normalized spectra of integrated fluorescence emission at 10 K of WSCP samples in buffer containing 50% glycerol; pigment composition: Chl *b* only (squares), Chl *a* only (stars) and Chl *a*:Chl *b* at ratios of 4.2:1 (triangles) and 2.6:1 (circles). Excitation wavelength: 632 nm. The black cross positioned near the emission maximum of Chl *b* only WSCP indicates the confidence interval of the integrated fluorescence spectrum.

sum of the spectra of WSCP containing Chl *a* only and Chl *b* only. This phenomenon is interpreted as to reflect the formation of Chl *a*/Chl *b* heterodimer forms which exhibit stronger contributions of fluorescence emission at 685 nm than a mixture of WSCP complexes containing only Chl *a*/Chl *a* and Chl *b*/Chl *b* homodimers, due to a larger oscillator strength of the lower exciton state in Chl *a*/Chl *b* heterodimers.

The normalized integrated emission spectra of the different WSCP samples measured at 10 K are shown in Figure 5. As expected, the shape of the bands is significantly sharpened in comparison to the room temperature spectra shown in Figure 2. Especially the spectra of mixed Chl *a*:Chl *b* WSCP do not exhibit significant fluorescence at 665−675 nm where strong emission is found at room temperature. Only in the sample with a Chl *a*:Chl *b* ratio of 2.6:1 there is a rather weak fluorescence visible at 670 nm (±3 nm). The main emission is located at 685 nm. On the basis of these findings, a significant amount (>5%) of uncoupled Chl *b* or Chl *b* homodimers, which show fluorescence peaking at 668 nm at 10 K (see Figure 5, black squares and Figure 6 panel B), can be ruled out in WSCP containing Chl *a*:Chl *b* at a ratio of 2.6. For WSCP containing Chl *a*:Chl *b* at a ratio of 4.2 the emission spectra show that the contribution of uncoupled Chl *b* or Chl *b* homodimers is <1%.

The emission bands at 10 K presented in Figure 6 are well fit by a sum of Gaussians. The use of Gaussian functions in the fit of low temperature spectra in contrast to that of Lorentzian functions at room temperature (see Figure 2) takes into account that at low temperatures the spectra are more likely dominated by inhomogeneous broadening. In the wavelength region <700 nm the main emission bands at 668 nm of WSCP containing Chl *b* only (Figure 6B) and at 685 nm of WSCP containing Chl *a* only (Figure 6A) or Chl *a* and Chl *b* at ratios of 4.2:1 (Figure 6C) and 2.6:1 (Figure 6D)) are shown to be the composite of two sharp Gaussians. Furthermore, in all samples a smaller band exists with a peak at longer wavelength and markedly broader fwhm.

Since the spectral absorption properties of our WSCP samples were found to be dominated by the strongly coupled dimers [1,2] it appears most reasonable to assign the major band in the deconvoluted 10 K emission spectra to this pigment array. The slightly red-shifted minor bands (see Figure 6) cannot be explained straightforwardly at present. These bands might represent phonon sidebands or could indicate heterogeneity. Questions also arise as to the origin of the minor bands observed at 685 nm for Chl *b* homodimers and at around 692−702 nm for the other complexes. These bands with markedly larger fwhm values can be assigned to vibrational bands as will be outlined in the discussion.

A more complex situation is expected for WSCP containing Chl *a* and Chl *b* because in this case the ensembles contain complexes with homo- and heterodimers. Since the spectra of WSCP containing Chl *a* and Chl *b* can be fitted by the same number of bands, Chl *a*/Chl *b* heterodimers and Chl *a*/Chl *a* homodimers exhibit quite similar emission spectra at 10 K (see Figure 6).

The normalized integrated fluorescence spectra $F(\lambda) = \int_0^\infty F(\lambda,t)\, dt$ of Figures 2–6 nicely complement our former studies on the absorption and CD spectra of WSCP complexes.[1,2] Information on the fate of the lowest excited singlet states ^{1}Chl* of WSCP complexes is obtained by intersection of the data set along the time axis at constant wavelength (see Figure 1, upper right panel).

Lifetimes of Excited States. At room temperature all samples exhibit a monoexponential decay kinetics with time constants of 5.2 ns for samples containing Chl *a* alone or Chl *a*:Chl *b* mixtures and of 4.8 ns for Chl *b* only WSCP in buffer solutions containing 50% glycerol. Similar kinetics were observed in the presence of sucrose and imidazole (data not shown).

Figure 7 shows typical traces of fluorescence decay curves F(λ,t) monitored at 10 K.

The data of the left panel of Figure 7 reveal that at 10 K the fluorescence decay kinetics are slower in Chl *b* only WSCP (at 668 nm) than in WSCP containing Chl *a*:Chl *b* mixtures or Chl *a* only WSCP at 685 nm (see Figure 10). Furthermore, the decay is not strictly monoexponential and exhibits fast decay components in the short wavelength region (663 nm in WSCP containing Chl *b* only, 665 nm in WSCP containing mixtures of Chl *a*: Chl *b*). At longer wavelengths pronounced rise kinetics are discernible (see traces on the right panel of Figure 7). The time constant of this very fast rise component is 80−120 ps in all WSCP samples at 10 K and will be designated "100 ps component" throughout this paper.

An accurate fit of the decay curves requires at least 3 decay components (see Figure 8).

In order to obtain more detailed information the data were analyzed by deconvolution into decay associated spectra (DAS). For this reason the 10 K fluorescence decay curves of different wavelength sections were fitted together (global fit) with lifetime values τ_j as linked parameters and wavelength-dependent pre-exponential factors $a_j(\lambda)$ (nonlinked parameters). The results of such analyses according to eq 1 are usually plotted as graphs of $a_j(\lambda)$ for all wavelength-independent lifetimes τ_j representing so-called decay associated spectra (DAS), thus showing the energetic position of individual decay components. For further details on the data analysis see Vasil'ev et al.[34]

Figure 8 presents the characteristic DAS gathered from measurements performed at 10 K on WSCP containing Chl *a*:Chl *b* with a ratio of 2.6:1 (left panel) and Chl *b* only WSCP (right panel). It was found (data not shown) that the DAS of Chl *a* only WSCP or WSCP containing Chl *a*:Chl *b* at a ratio of 4.2:1 are very similar to the data presented in the left panel of Figure 8 with the only difference that the emission at 660 − 670 nm is even smaller in comparison to WSCP containing Chl *a*:Chl *b* at a ratio of 2.6:1.

The traces were fitted with three time constants: 6.0 (±0.3) ns, 2.5 (±0.4) ns, and 120 (±20) ps (left panel) and 7.0 (±0.3) ns, 3.6 (±0.4) ns, and 80 (±20) ps (right panel).

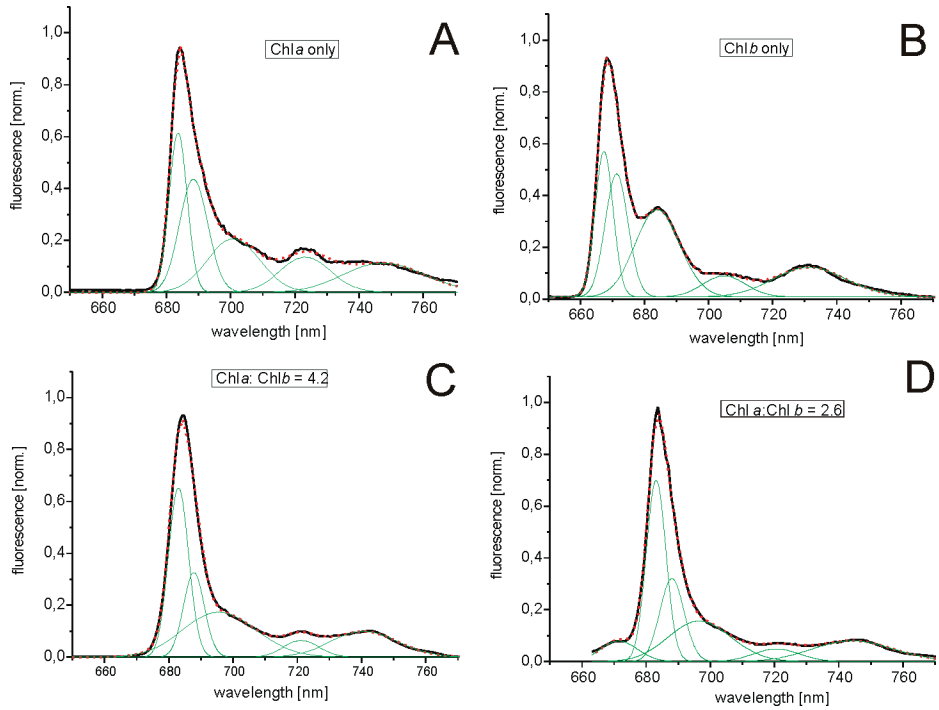

Figure 6. Gaussian fits of the normalized emission spectra of Figure 5 for WSCP samples containing Chl *a* only (A), Chl *b* only (B) and Chl *a*:Chl *b* at ratios of 4.2:1 (C) and 2.6:1 (D) at 10 K. The dotted curves show the sum of all Gaussian bands in comparison to the measured fluorescence (full-lined curves). Fits were performed in the frequency domain and the data were transformed to the wavelength domain.

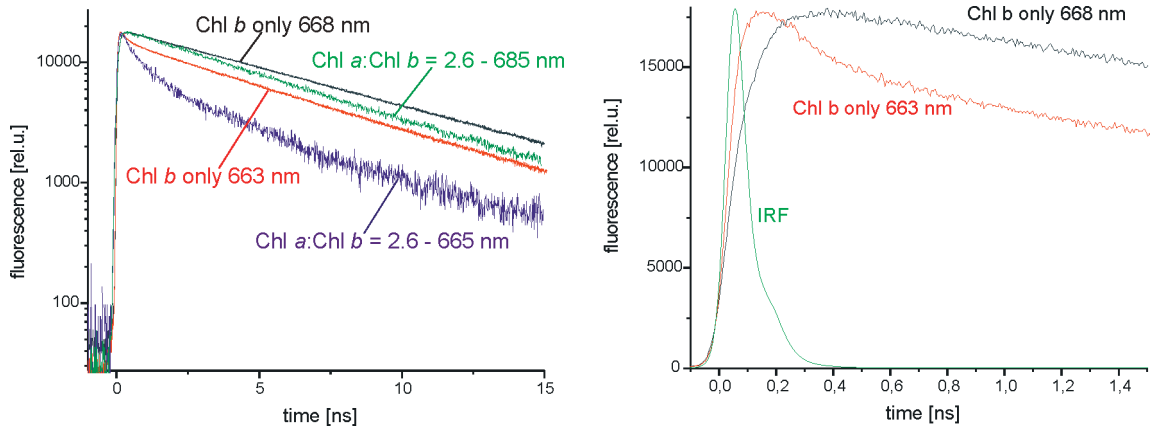

Figure 7. Left panel: Semilogarithmic plot of the fluorescence decay measured at 10 K on WSCP samples containing Chl *b* only (monitored at 663 and 668 nm) and WSCP containing Chl *a* and Chl *b* at a ratio of 2.6:1 (monitored at 665 and 685 nm). Excitation wavelength: 632 nm. The curves are normalized and therefore the S/N ratio is different. All measurements at 10 K were performed on frozen solutions containing 50% glycerol. Right panel: Linear plot of the fluorescence transients at 663 and 668 nm of Chl *b* only WSCP and the IRF.

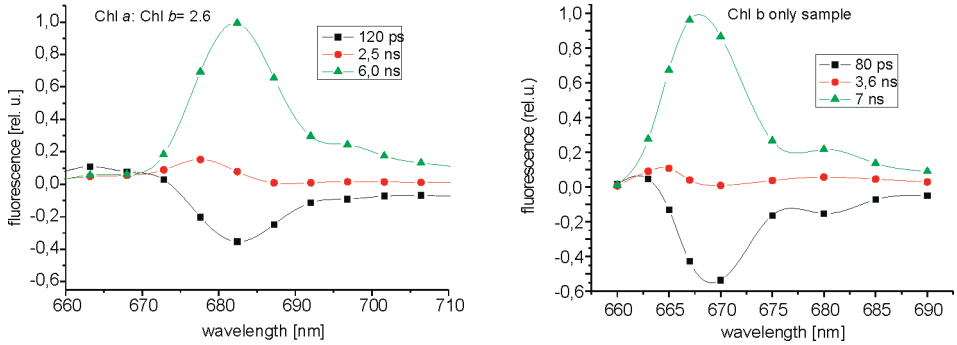

Figure 8. Decay associated spectra (DAS) at 10 K of WSCP samples containing either Chl *a*:Chl *b* at a ratio of 2.6:1 (left panel) or Chl *b* only (right panel) in frozen buffer solution containing 50% glycerol.

The DAS of both sample types are characterized by a component with a pronounced negative amplitude and a time constant in the order of 100 ps at 10 K ("100 ps component"). The negative sign of this component indicates that it reflects the rising transient population of the low energy emitter state. This process is much slower than the relaxation from the

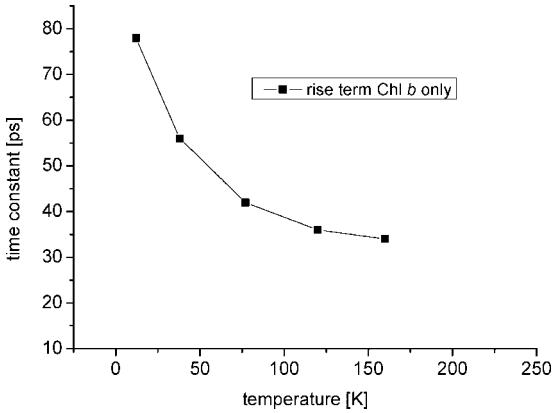

Figure 9. Time constant of the "100 ps component" in WSCP containing Chl *b* only as a function of temperature.

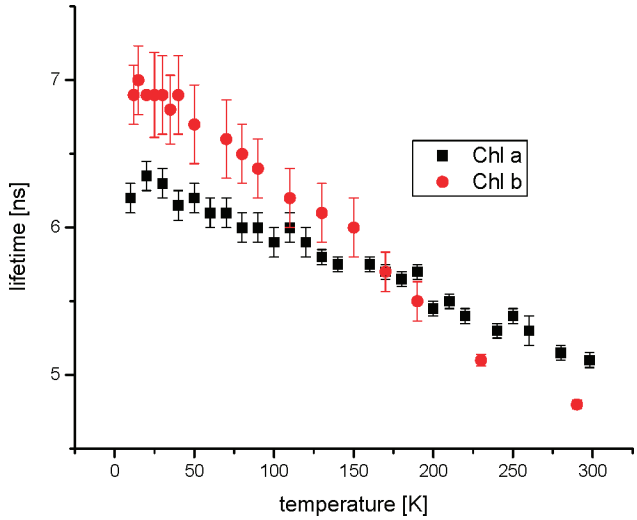

Figure 10. Lifetime of the dominant decay component as a function of temperature of WSCP containing Chl *a* only (monitored at 684 nm, filled squares) and Chl *b* only (monitored at 667 nm, filled circles) in buffer containing 50% glycerol.

upper to the lower exciton state (<1 ps) resolved in our former study.[1] In order to obtain information on the possible origin of this component we measured its temperature dependence. The data obtained for Chl *b* only WSCP are shown in Figure 9:

The "100 ps component" is found to become even faster at higher temperatures and reaches a value of 35 ps at 160 K. Concomitantly the amplitude of this component becomes smaller (data not shown) until this component is below the detection limit at higher temperatures than 160 K. On the basis of this finding, we concluded that a protein relaxation process might be responsible for these kinetics as will be outlined in the discussion.

A temperature dependence arises also for the ns decay as reflected by the room temperature values of 5.2 and 4.8 ns for WSCP containing Chl *a* only and Chl *b* only, respectively, and the corresponding time constants of 6.2 ns (Chl *a* only) and 7.0 ns (Chl *b* only) for the dominating kinetic component at 10 Kelvin.

These numbers readily show that Chl *a* only and Chl *b* only WSCP differ in the temperature dependence of their excited singlet state lifetimes. The complete temperature dependence of the dominating decay component of Chl *a* only and Chl *b* only WSCP is shown in Figure 10.

Discussion

The results of the present study unambiguously show that the lifetime of the excited singlet states of the chlorophyll molecules remains virtually unaffected upon binding to the matrix of the class II WSCP polypeptide. In particular, the formation of an excitonically strongly coupled dimer in the open sandwich form that is confirmed by both spectral analysis [1,2,22] and X-ray diffraction crystallography[23] does not lead to a quenching configuration. In the following the nature of the emission, excited singlet state dynamics and implications of these findings will be discussed.

Spectral Band Assignment in the Time-Integrated Fluorescence Spectrum. The linear absorption spectra could be described by considering only dimers with strong excitonic coupling.[1,2] The transient absorption data suggested the existence of a small fraction of weakly coupled dimers in addition to the majority of strongly coupled dimers.[1]

If one assumes that the site energies of the strongly and weakly coupled Chl homodimers in each WSCP complex are not markedly different, the emission band is anticipated to be slightly shifted by about 5 nm to longer wavelengths in the strongly coupled Chl dimers.[1,2,22] The spectral deconvolution into Gaussians shows that the overall spectrum in the Q_y region of 0−0 transitions at 10 K can be described as the composite of three bands. The fluorescence spectra in Figure 6 A and B reveal the existence of a major band at 684 nm and a smaller "satellite" at 689 nm for Chl *a* only and a major band at 667 nm and its minor "satellite" at 672 nm for Chl *b* only WSCP.

We ascribe the bands peaking at 667 and 684 nm to emission from the low-energy exciton state of strongly coupled homodimers in WSCP containing Chl *b* or Chl *a*, respectively, because of the spectral dominance of these forms. Accordingly, the "satellite" bands that emerge at the long wavelength side of the major bands might reflect the emission from the minority of weakly coupled dimers found in the transient absorption (see ref 1) but this would imply unreasonably large Stokes shifts in the order of 10 nm. This value is difficult to reconcile within the framework of the typically weak electron−phonon coupling observed in many photosynthetic antenna complexes, which suggests a quasi-resonant location of the absorption and the corresponding fluorescence bands with Stokes shifts in the range 0.5−1.0 nm.[35−38] The Huang–Rhys factor $S = 0.8$ estimated from the temperature dependence of the linear absorbance spectrum of WSCP[2] clearly shows that also in this complex the electron–phonon coupling is weak. This effect should be even more pronounced for the lower exciton level, because a decrease of the electron−phonon coupling strength is expected in the case of strong excitonic coupling.[39] Therefore, an identification of the "satellite" bands arising from the exciton transactions is even less likely.

Therefore, we favor an assignment to vibrational sidebands because the shape of fluorescence bands at low temperature is expected to be strongly asymmetric due to electron−phonon coupling (see ref 37). The appearance of a 80 cm^{-1} mode in the vibrational side bands has been attributed to an intra dimer mode that varies the mutual distance between the two monomers.[40−42] However, it was also reported for the low energy state of the CP 29 antenna that is supposed to be monomeric.[43] A more detailed investigation of band positions and electron−phonon coupling requires the application of site-selective spectroscopies like hole-burning and/or fluorescence line-narrowing.

Apart from the assignment of the major bands at 667 and 684 nm and the accompanying "satellites" at 672 and 689 nm in Chl *b* and Chl *a* only WSCP, respectively, the origin of another band remains to be clarified. The Gaussian fit reveals that this band is positioned at about 685 and 702 nm in Chl *b* only WSCP and in

Chl *a* only WSCP, respectively, and characterized by significantly larger fwhm values. Interestingly, in both homodimeric WSCP complexes (Chl *a* only and Chl *b* only) the peak position of this band is shifted by 18 nm to the red compared with the major bands at 667 nm (Chl *b*) and 684 nm (Chl *a*) (vide supra). This shift corresponds to energies of about 400 cm^{-1} and could reflect a vibrational effect. Intramolecular vibrational modes of isolated Chl *a* molecules form an almost continuous spectrum in the frequency range from ~240 to ~1700 cm^{-1}, while the most pronounced modes are located at around 700 and 1200 cm^{-1}.[43−45] However, the intensities of the WSCP vibrational bands at about 400 cm^{-1} appear to be significantly enhanced in comparison to isolated Chl molecules in solution.

On the basis of these considerations, it seems attractive to assume that the broad minor bands at 685 and 702 nm could originate from a special mode of vibrational coupling. The coupling to an intermolecular pigment vibration could also rationalize the significantly larger fwhm values assigned by the present Gaussian fit. By comparing parts A and B of Figure 6, it becomes obvious that the 400 cm^{-1} mode is more intense in Chl *b* than in Chl *a* homodimers, despite the same geometrical dimer structure and a very similar electronic structure of Chl *a* and Chl *b*. The origin of this difference is not known but could reflect the sample heterogeneity in Chl *b* only WSCP that is seen as a very minor absorbance peak at 680 nm.[1,2] The origin of this heterogeneity is unknown but we are confident that it is not responsible for the majority of the bands at 685 and 702 nm in Chl *b* only and Chl *a* only WSCP, respectively, because of the striking similarity of the properties of these bands (e.g., the same extent of band shift relative to the major bands at 667 and 684 nm of Chl *b* only and Chl *a* only samples, respectively) in all WSCP samples analyzed in this study.

The results of Figure 6 show that the WSCP samples containing mixtures of Chl *a* and Chl *b* exhibit a rather small (2.6:1 sample) and no detectable (4.2:1 sample) emission in the wavelength region of Chl *b* (667 nm). This finding is somehow surprising because the extent of Chl *b* homodimers is expected to be about 3.5% and 8% in WSCP containing Chl *a*:Chl *b* at ratios of 4.2 and 2.6, respectively, according to formation of tetramers with two chlorophylls by a statistical binding of monomers containing Chl *a* and/or Chl *b* and two empty subunits. Therefore, heterodimers seem to be preferentially formed. The underlying mechanism for this phenomenon is not known.

Fluorescence Lifetime and Temperature Dependence. The time-resolved fluorescence transients of Figure 7 and the DAS data analysis reveal that the excited singlet state decay at 10 K of the WSCP samples in buffer containing 50% glycerol can be described by triphasic kinetics with time constants of 80−120 ps ("100 ps component"), 2−3 ns and a dominating component of 6−7 ns. The "100 ps component" and the "6−7 ns kinetics" exhibit characteristic temperature dependencies (see Figures 9 and 10). At room temperature, the decay of all samples is monoexponential.

The 2−4 ns component is characterized by a very small amplitude and a blue shift compared to the main emission. It seems possible that this component is caused by sample heterogeneity, but alternative explanations cannot be ruled out. Since the extent of this component is very small, and therefore its properties are difficult to resolve, we will refrain from any speculations on its nature and will focus our considerations on the "100 ps component" and the dominant 6−7 ns kinetics.

The spectral properties of the fluorescence emission have been explained within the framework of strongly coupled Chl dimers that is used also in the following.

At 10 K only the lower exciton state is populated because the energy gap between both states is of the order of 100 cm^{-1} in the homodimers, and even larger in Chl *a*/Chl *b* heterodimers;[1,2] i.e., the population probability of the upper exciton state is $<10^{-5}$ in a Boltzmann equilibrium. The exciton relaxation was shown to take place in <1 ps[1] so that the emission at 10 K with lifetimes of 6−7 ns takes place exclusively from the lower exciton state (the subpicosecond equilibration is far beyond the time resolution of our fluorescence measurements).

An unexpected and interesting feature is the "100 ps component" that can be detected when the measurements are performed at temperatures below 160 K. It is observed in all samples analyzed in this study and exhibits a marked temperature dependence as is illustrated in Figure 9 for Chl *b* only WSCP. The time constant of this component decreases from 80 ps at 10 K to 35 ps at 160 K for this sample. These values are far too large to be assignable to intradimer excitation energy transfer (see above), while they compare favorably to the effective dephasing times determined for the terminal (fluorescing) electronic states of trimeric LHC II [36,46] and CP29.[47] In the latter case, the widths of spectral holes burnt into the lowest electronic state were shown to exhibit a temperature dependence that is characteristic for pure dephasing of electronic excitations in amorphous protein matrices with dephasing times of ~400 and ~70 ps at 4.2 and 10 K, respectively. Such processes are usually described by a coupling of the pigment's electronic transition to a distribution of asymmetric double well potentials of the surrounding protein matrix [48,49] where each potential well represents a different conformational substate of the pigment−protein system and the observed dephasing is attributed to tunneling processes within the double well potentials at low temperatures. In analogy to these processes we propose that the "100 ps component" represents a protein relaxation process in the excited electronic state. This idea would also explain the pronounced temperature dependence of the "100 ps component". A change at ~120 K correlates with the glass transition, i.e., the onset of thermally activated conformational flexibility as recently shown for PS II membrane fragments.[50] Based on these observations it seems likely to assign this component to a protein relaxation process that can be described by a transition within a double well potential curve as is schematically shown in Figure 11. The results of the DAS analyses of the data depicted in Figure 8 reveal that the "100 ps component" exhibits a rather small positive amplitude in the range of 660−665 nm and a pronounced negative amplitude with a peak near 668 nm in Chl *b* only WSCP and at about 685 nm in samples containing Chl *a*:Chl *b* at a ratio of 2.6:1 (see Figure 8). This general feature can be simulated by a model with a double well potential for both the ground and excited state (see Figure 11, left panel) and a relaxation kinetics of 80−120 ps at 10 K as is illustrated by the calculated DAS on the right panel of Figure 11 for WSCP containing Chl *b* only which fits the experimental data of Figure 8 (right panel) (for details regarding the simulation, see ref 51). This calculation is based on the assumption that the transition probability from the 663 nm state to the ground-state is lower than that from the 668 nm state by a factor of 6.

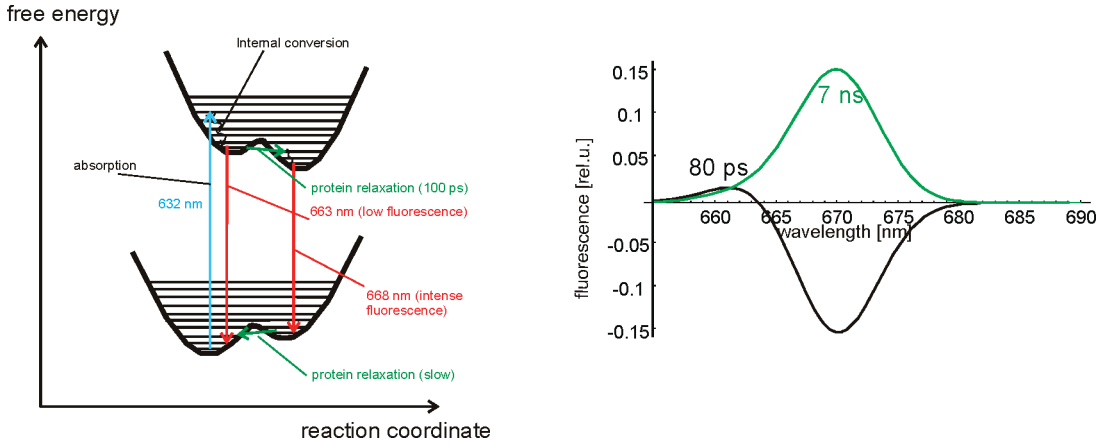

Figure 11. Left panel: Simplified 1-dimensional scheme of the free energy surfaces of a two-level system for the ground and excited state of WSCP containing Chl *b* only. Right panel: simulated DAS of a system consisting of two states with emissions at 663 and 668 nm connected via a conformational transition of the excited-state with a rate constant of (100 ps)$^{-1}$ and no conformational relaxation of the ground-state during the lifetime of the excited singlet state. The probability of fluorescence emission is assumed to be smaller for the 663 nm state in comparison to the 668 nm state.

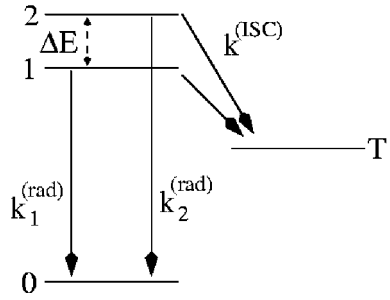

Figure 12. Scheme of the radiative k_i^{rad} (i = 1 or 2) and nonradiative $k^{(ISC)}$ decay of exciton states 1 and 2 (for further details, see text).

A "100 ps component" was not detected by the pump−probe experiments of ref 1 because these were performed at room temperature and in a time window of 30 ps. On the other hand, processes faster than 10 ps cannot be resolved in the fluorescence measurements shown in the study presented here.

The time-resolved measurements revealed that the 6−7 ns lifetime at 10 K of the dominating decay component almost linearly decreases with increasing temperature (see Figure 10). In marked contrast to the "100 ps component" this temperature dependence is not caused by protein relaxation but emerges from the energy levels of the two exciton states of the strongly coupled dimer.

A consistent explanation of the behavior is achieved when the dimer system satisfies two conditions: (i) thermal equilibration is much faster than the decay of the excited-state populations and (ii) the rate constants of decay differ for the upper and the lower exciton states.

A simplified scheme is shown in Figure 12.

The inverse lifetime $1/\tau$ of this system is obtained by the relation

$$\frac{1}{\tau} = k = \frac{k_1 + k_2 \exp(-\Delta E/k_B T)}{1 + \exp(-\Delta E/k_B T)} \qquad (2)$$

where ΔE is the energy gap between the upper and the lower exciton state 2 and 1 of the dimer, respectively, T the absolute temperature and k_B the Boltzmann constant. The Boltzmann factor $\exp(-\Delta E/k_B T)$ takes into account a fast equilibration of excitons between the upper and lower level prior to radiative or nonradiative decay. The rate constants k_1 and k_2 comprise the sum of the radiative and nonradiative decay rates of the two exciton levels, i.e.

$$k_i = k_i^{(rad)} + k_i^{(non\text{-}rad)} \qquad (3)$$

Inspection of the Einstein coefficients reveals that the radiative rate constant $k_i^{(rad)}$ is proportional to the oscillator strength of the optical transition from excited state i to the ground state. Hence, in WSCP complexes with a strongly coupled open sandwich dimer arrangement of the two Chl molecules, the radiative lifetimes $k_i^{(rad)}$ of the exciton states i = 1, 2 differ strongly due to their different oscillator strengths. Calculations reveal that the oscillator strength of the upper exciton state i = 2 is larger by factors of 8−10 than that of the lower exciton state i = 1 (in marked contrast to excitonic pigment coupling in antenna systems and reaction centers RCs/PSs, for a discussion see refs [1,2]). When using the value of $k_i^{(rad)} = 6.8 \times 10^7$ s^{-1} for monomeric Chl *a* in solution[52] the values of $k_1^{(rad)}$ and $k_2^{(rad)}$ are estimated to be 1.8×10^7 s^{-1} and 1.4×10^8 s^{-1}, respectively. In solutions of monomeric Chl *a* the rate constant $k_i^{(non\text{-}rad)}$ corresponds to $k^{(ISC)}$ for intersystem crossing with a value of 1.3×10^8 s^{-1}.[52] On the basis of the idea that $k^{(ISC)}$ is independent of temperature and not affected by binding to the protein matrix, values of 1.4×10^8 s^{-1} and 2.7×10^8 s^{-1} are obtained for k_1 and k_2, respectively. When using these values, decay times of 7.2 ns at 10 K and 5.5 ns at 300 K are obtained for Chl *a* only WSCP, which explain qualitatively the observed experimental decrease from 6.2 ns at 10 K to 5.2 ns at 300 K (see Figure 10). A more quantitative theoretical analysis using our exciton model [1,2] is in progress.

Based on these considerations it is also expected that the lifetime of the dominating "6−7 ns kinetics" at 10 K is larger for Chl *a* homodimers than for Chl *a*/Chl *b* heterodimers because the oscillator strength of the lower exciton state in the latter dimer is larger by a factor of about four than that of the homodimer (see Figure 8 of ref 1). This effect is really observed; i.e., the lifetimes at 10 K are 6.2 and 6.0 ns for the Chl *a* homodimer and the sample containing Chl *a* and Chl *b* at a ratio of 2.6:1, respectively.

A somewhat surprising result is the difference of the temperature dependence of the ^{1}Chl* lifetime in Chl *a* only and Chl *b* only WSCP (see Figure 10). This difference indicates that besides the exciton oscillator strength/population effect

described above, other factors have to be considered as well. One possibility could be a different temperature dependence of the nonradiative decay rate constants $k_i^{(non\text{-}rad)}$ in Chl *a* and Chl *b* homodimers. The latter idea is investigated in detail in a forthcoming theoretical study.

Mechanistic Considerations on the Stability of Chl Bound to WSCP. The results of the present study unambiguously show that the lifetime of the lowest excited singlet state of Chl is nearly the same in monomeric solution and when bound to the class II WSCP protein matrix. Accordingly, the highly protective role to pigment degradation and the markedly diminished potential of singlet oxygen formation by Chl bound to WSCP cannot be explained by a reduced probability for ^{3}Chl formation or by a drastic quenching of ^{1}Chl*, in contrast to the situation of the single Chl molecule that is bound to the Cyt b_6/f complex. In the latter case the lifetime is shortened by a factor of about 20,[25−27] thus suppressing ^{3}Chl formation down to less than 5% of the value of diluted Chl solutions. Also, the formation of $^1\Delta_gO_2$ is diminished by comparable values if Chl is bound to Cyt b_6/f. On the basis of our findings, this mode of protection can be excluded for WSCP. Therefore, the only reasonable explanations are the following ones:

(i) In the WSCP protein a high diffusion barrier exists that drastically reduces the interaction between Chl and O_2 as suggested by Horigome et al.[23] This mode of protection does not require the existence of carotenoids as protective pigments that are in van der Waals contact with the Chls.

(ii) Compared to the "free" pigments the lifetime of the ^{3}Chl state might be markedly reduced in WSCP even in the absence of carotenoids, thus suppressing the formation of $^1\Delta_gO_2$. At present, a reasonable underlying mechanism for this type of ^{3}Chl quenching is not known.

At first glance, it is surprising that Chl binds to WSCP in the form of open sandwich dimers with strong excitonic coupling because the arrangement is not quenching. Therefore, it seems more likely that this pigment array is favored by a structure of the environmental protein matrix that suppresses $^1\Delta_gO_2$ through establishing a high diffusion barrier or by quenching ^{3}Chl. The "diffusion barrier" hypothesis is in line with conclusions gathered from data on the structure of class II WSCP containing 4 Chl molecules.[23]

This interesting mechanism of protecting Chl from degradation and the diminished singlet oxygen formation will be addressed in future studies.

Acknowledgment. The financial support by the German Research Foundation (DFG) through collaborative research center Sfb 429 (TP A1 and A9) and Pa 324/8-1 (to H.P.) is gratefully acknowledged.

References and Notes

(1) Theiss, C.; Trostmann, I.; Andree, S.; Schmitt, F. J.; Renger, T.; Eichler, H. J.; Paulsen, H.; Renger, G. *J. Phys. Chem. B* **2007**, *111*, No. 46, 13325.

(2) Renger, T.; Trostmann, I.; Theiss, C.; Madjet, M. E.; Richter, M.; Paulsen, H.; Eichler, H. J.; Knorr, A.; Renger, G. *J. Phys. Chem. B* **2007**, *111*, No. 35, 10487.

(3) Renger, G. In *Primary processes of photosynthesis: Basic principles and apparatus*; Renger, G., Ed.; RSC Publ.: Cambridge, U.K., 2008; Vol. I, p 5.

(4) Ke, B. *Photosynthesis*; Kluwer Academic: Dordrecht, The Netherlands, 2001; Vol. 10.

(5) Law, C.; Cogdell, R. In *Primary processes of photosynthesis: Basic principles and apparatus*; Renger, G., Ed.; RSC Publ.: Cambridge, U.K., 2008; Vol. I, p 205.

(6) Mimuro, M.; Kobayashi, M.; Murakami, A.; Tsuchiya, T.; Miyashita, H. In *Primary processes of photosynthesis: Basic principles and apparatus*; Renger, G., Ed.; RSC Publ.: Cambridge, U.K., 2008; Vol. I, p 261.

(7) van Amerongen, H.; Croce, R. *in Primary processes of photosynthesis: Basic principles and apparatus*; Renger, G., Ed.; RSC Publ.: Cambridge, U.K., 2008; Vol. I, p 329.

(8) Parson, W. *in Primary processes of photosynthesis: Basic principles and apparatus*; Renger, G., Ed.; RSC Publ.: Cambridge, U.K., 2008; Vol. II, p 57.

(9) Setif, P.; Leibl, W. *in Primary processes of photosynthesis: Basic principles and apparatus*; Renger, G., Ed.; RSC Publ.: Cambridge, U.K., 2008; Vol. II, p 147.

(10) Renger, G. *in Primary processes of photosynthesis: Basic principles and apparatus*; Renger, G., Ed.; RSC Publ.: Cambridge, U.K., 2008; Vol. II, p 237.

(11) Polivka, T.; Sundstrom, V. *Chem. Rev.* **2004**, *104*, 2021.

(12) Schmidt, K.; Fufezan, C.; Krieger-Liszkay, A.; Satoh, H.; Paulsen, H. *Biochemistry* **2003**, *42*, 7427.

(13) Satoh, H.; Uchida, A.; Nakayama, K.; Okada, M. *Plant Cell Physiol.* **2001**, *42*, 906.

(14) Satoh, H.; Nakayama, K.; Okada, M. *J. Biol. Chem.* **1998**, *46*, 30568.

(15) Downing, W. L.; Mauxion, F.; Fauvarque, M. O.; Reviron, M. P.; de Vienne, D.; Vartanian, N.; Giraudat, J. *Plant J.* **1992**, *2*, 685.

(16) Reviron, M.; Varantian, N.; Sallantin, M.; Huet, J.; Pernollet, J.; de Vienne, D. *Plant Physiol.* **1992**, *100*, 3–1486.

(17) Annamalai, P.; Yanagihara, S. *J. Plant Physiol.* **1999**, *155*, 2–226.

(18) Nishio, N.; Satoh, H. *Plant Physiol.* **1997**, *115*, 841.

(19) Reinbothe, C.; Satoh, H.; Alcaraz, J.; Reinbothe, S. *Plant Physiol.* **2004**, *134*, 4–1355.

(20) Matile, P.; Schellenberg, M.; Vicentini, F. *Planta* **1997**, *201*, 1–96.

(21) Kräutler, B.; Hörtensteiner, S. In *Chlorophylls and bacteriochlorophylls*; Grimm, B., Porra, R. J., Rüdiger, W., Scheer, H., Eds.; Springer: Dordrecht, The Netherlands, 2006; Vol. 25, p 237.

(22) Hughes, J. L.; Razeghifard, R.; Logue, M.; A. Oakley Wydrzynski, T.; Krausz, E. *J. Am. Chem. Soc.* **2006**, *128*, 3649.

(23) Horigome, D.; Satoh, H.; Itoh, N.; Mitsunaga, K.; Oonishi, I.; Nakagawa, A.; Uchida, A. *J. Biol. Chem.* **2007**, *282*, 6525.

(24) Beddard, G.; Porter, G. *Nature* **1976**, *260*, 366.

(25) Dashdorj, N.; Yamashita, E.; Schaibley, J.; Cramer, W.; Savikhin, S.; AF Dashdorj, N.; Yamashita, E.; Schaibley, J.; Cramer, W. A.; Savikhin, S. *J. Phys. Chem. B* **2007**, *111*, 51–14405.

(26) Cramer, W.; Zhang, H.; Yan, J.; Kurisu, G.; Yamashita, E.; Dashdorj, N.; Kim, H.; Savikhin, S. *in Primary processes of photosynthesis: Basic principles and apparatus*; Renger, G., Ed.; RSC Publ.: Cambridge, U.K., 2008; Vol. II.

(27) Dashdorj, N.; Zhang, H.; Kim, H.; Yan, J.; Cramer, W.; Savikhin, S. *Biophys. J.* **2005**, *88*, 4178.

(28) Vasil'ev, S.; Schrötter, T.; Bergmann, A.; Irrgang, K.; Eichler, H.; Renger, G. *Photosynthetica* **1997**, *33*, 553.

(29) Paulsen, H.; Rümler, U.; Rüdiger, W. *Planta* **1990**, *181*, 204.

(30) Hobe, S.; Fey, H.; Rogl, H.; Paulsen, H. *J. Biol. Chem.* **2003**, *278*, 5912.

(31) Bergmann, A.; Eichler, H.; Eckert, H.; Renger, G. *Photosynth. Res.* **1998**, *58*, 303.

(32) Bergmann, A. *Pikosekunden-Fluoreszenzspektroskopie mithilfe doppeltkorrelierter Einzelphotonendetektion zur Untersuchung Primärprozesse im Photosystem II*; Mensch & Buch: Berlin, 1999.

(33) Pieper, J.; Schödel, R.; Irrgang, K.; Voigt, J.; Renger, G. *J. Phys. Chem. B* **2001**, *105*, 7115.

(34) Vasil'ev, S.; Irrgang, K.; Schrötter, T.; Bergmann, A.; Eichler, H.; Renger, G. *Biochemistry* **1997**, *36*, 7503.

(35) Reddy, N.; van Amerongen, H.; Kwa, S.; van Grondelle, R.; Small, G. *J. Phys. Chem.* **1994**, *98*, 4729.

(36) Pieper, J.; Rätsep, M.; Jankowiak, R.; Irrgang, K.; Voigt, J.; Renger, G.; Small, G. *J. Phys. Chem. A* **1999**, *103*, 2412.

(37) Pieper, J.; Voigt, J.; Renger, G.; Small, G. *Chem. Phys. Lett.* **1999**, *310*, 296.

(38) Rätsep, M.; Freiberg, A. *Chem. Phys. Lett.* **2003**, *377*, 371.

(39) Rätsep, M.; Freiberg, A. *J. Lumin.* **2007**, *127*, 251.

(40) Johnson, S. G.; Small, G. J. *J. Phys. Chem.* **1991**, *95*, 471.

(41) Peterman, E. J. G.; van Amerongen, H.; van Grondelle, R.; Dekker, J. P. *Proc. Natl. Acad. Sci. U.S.A.* **1998**, *95*, 6128.

(42) Den Hartog, E. T. H.; Vacha, F.; Lock, A. J.; Barber, J.; Dekker, J. P.; Völker, S. *J. Phys. Chem.* **1998**, *102*, 9174.

(43) Rätsep, M.; Pieper, J.; Irrgang, K.; Freiberg, A. *J. Phys. Chem. B* **2008**, *112*, 110.

(44) Avarmaa, R.; Rebane, K. *Spectrochim. Acta A* **1985**, *41*, 1365.

(45) Gillie, J.; Small, G.; Golbeck, J. *J. Phys. Chem.* **1989**, *93*, 1620.

(46) Tietz, C.; Jelezko, F.; Gerken, U.; Schuler, S.; Schubert, A.; Rogl, H.; Wrachtrup, J. *Biophys. J.* **2001**, *81*, 556.

(47) Pieper, J.; Irrgang, K.-D.; Rätsep, M.; Voigt, J.; Renger, G.; Small, G. J. *Photochem. Photobiol.* **2000**, *71*, 574.

(48) Hayes, J. M.; Jankowiak, R.; Small, G. J. In *Persistent Spectral Hole-Burning: Science and Applications*; Moerner, W., Ed.; Springer: Berlin, 1988; p 153.

(49) Völker, S. In *Relaxation Processes in Molecular Excited States*; Fuenfschilling, J., Ed.; Kluwer Academic: Dordrecht, The Netherlands, 1989; p 113.

(50) Pieper, J.; Hauss, T.; Buchsteiner, A.; Baczynski, K.; Adamiak, K.; Lechner, R. E.; Renger, G. *Biochemistry* **2007**, *46*, 11398.

(51) Schmitt, F.-J.; Theiss, C.; Wache, K.; Fuesers, J.; Andree, S.; Handojo, A.; Karradt, A.; Kiekebusch, D.; Eichler, H. J.; Eckert, H.-J. *Proc. SPIE* **2006**, 638607/1.

(52) Parker, C.; Joyce, T. *Photochem. Photobiol.* **1967**, *6*, 395.

JP8024057